Third AO4ELT Conference - Adaptive Optics for Extremely Large Telescopes
Florence, Italy. May 2013
ISBN: 978-88-908876-0-4
DOI: 10.12839/AO4ELT3.13262

A STUDY OF PYRAMID WFS BEHAVIOUR UNDER IMPERFECT ILLUMINATION

Valentina Viotto[1,a], Demetrio Magrin[1], Maria Bergomi[1], Marco Dima[1], Jacopo Farinato[1], Luca Marafatto[12] and Roberto Ragazzoni[1]

[1]INAF – Osservatorio Astronomico di Padova, Vicolo dell'Osservatorio 5, 35122, Padova, Italy

[2] Università degli Studi di Padova, Dipartimento di Fisica e Astronomia, Vicolo dell'Osservatorio 3, 35122, Padova, Italy

Abstract. Even if still nowadays it's often referred to as an "innovative concept", the Pyramid wavefront sensor has been technologically demonstrated at the TNG in Canary Island years ago. It was again tested in laboratory and on the sky in the framework of the development of MAD, led by ESO, and recently succeeded to achieve outstanding performances at the LBT telescope. At the same time, several theoretical development raised novel features of this device, and actual measurements in the framework of Pyramir experimentally confirmed the better behaviour of this sensor with respect to the Shack-Hartmann in terms of noise propagation in closed loop, as previously analytically predicted. After a brief review of previous works, which revealed or demonstrated some peculiarities of this type of wavefront sensor with respect to other systems, we present a generalization of the photon efficiency and the non-linearity estimations of such sensor. The aim of this study is to devise, through analytical computations and Fourier wave-optics propagation simulations, the behaviour of the Pyramid wavefront sensor when not-ideal illumination conditions, such as faint-end sources and partial wavefront correction, are purposely applied. In the same framework, the effects of introducing a pyramid modulation are discussed too.

1. Introduction

The pyramid wavefront sensor (PWFS) has been proposed in 1996 [1] as an alternative to other types of wavefront derivative measuring WFSs. The first on-sky loop was closed on AdOpt@TNG [2] in the Canary Island in 2000, while paper studies on the PWFS peculiarities were being carried on by different authors [3], [4]. Some of the properties devised in those papers, like the gain in limiting magnitude with respect to the Shack-Hartmann WFS and the non-linearity reconstruction error issue, will be discussed in more detail. The potentiality of the PWFS were confirmed also in MCAO configuration during the MAD experiment at the VLT [5], while, in the latest years, the successful results of the First Light Adaptive Optics (FLAO) system at the 8m telescope LBT [6] gave the final consecration of the PWFS as one of the most powerful and promising wavefront sensors concept for AO.

a e-mail : valentina.viotto@oapd.inaf.it

The goal of this paper is to discuss, in a descriptive manner or with analytical computations and simulations, the behavior of the Pyramid wavefront sensor when not-ideal illumination conditions are applied. That means that the system is pushed either to its extreme limits in terms of faint-end reference sources or to partial wavefront correction conditions.

2. Very Linear WFS

The analysis presented in the following has been carried on in the framework of a study on the Global MCAO (GMCAO) technique [7], being carried on for ESO. This AO technique requires, for the wavefront sensing, for sensors characterized by both a high sensitivity and a very linear response in the slopes measurements. Fig. 1 introduces the VL-WFS concept, which is the WFS which processes the light coming from each NGS in the GMCAO system [8].

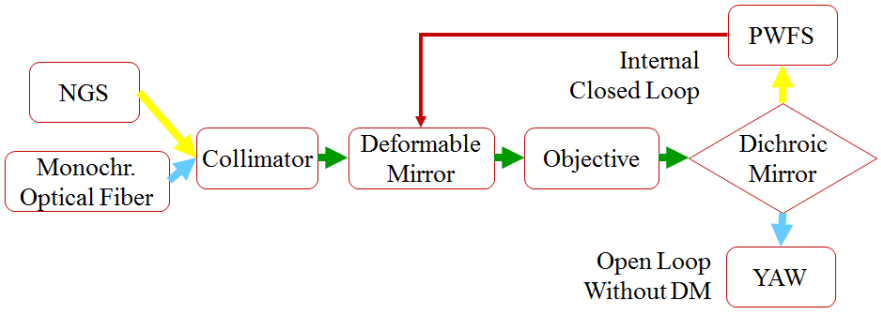

Fig. 1 VL-WFS scheme

There are two WFSs in a single arm, a PWFS is working in a locally closed loop with a DM, to take advantage of the increase in the sensitivity, and another WFS, in the scheme it's a YAW WFS [9], is working in open loop directly looking at the shape of the mirror (this is possible because of the large linearity range of this kind of WFS). The residual measurements of the pyramid are combined with the YAW measurements. This means that the pyramid is working in closed loop with a correcting device which can allow for a wavefront correction only up to certain spatial scale, corresponding to a radial order n. The PWFS will still measure higher orders aberrations, with a certain non-linearity error that we tried to estimate.

3. Re-imaging optics errors

In this paragraph are presented some effects of not-perfect illumination due to the re-imaging optics, which have been discussed in the past, but which are not part of this analysis since they are not strictly related only to PWFS.

A distortion which could arise on the pupils image, e.g., translates into a bad wavefront reconstruction. If we consider a four *pure* pupils image (that is to say that's an ideal image without any aberration or diffraction effect) and apply a distortion coordinates transformation, the WFS will detect a non-existing wavefront, shown in Fig. 2, with a shape which recalls the astigmatism. This effect is often small and in principle it can be quantified and corrected as a static aberration of the AO system.

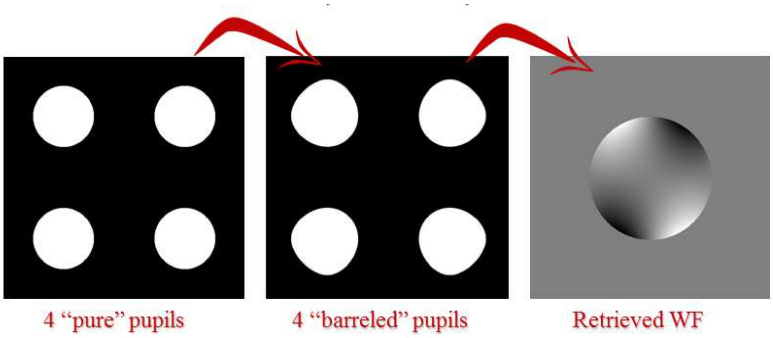

Fig. 2 Example of the effect of a distortion pattern applied onto the 4 pupil images of a PWFS.

Another example, discussed in [10], is the re-imaging optics MTF, the hampering factor of each spatial frequency in the image. High-spatial frequencies are imaged with a smaller gain than the low-frequencies pattern. Each Zernike polynomial might be associated to a particular spatial frequency, inversely proportional to the number of zeroes. High-order polynomials, then, are seen with a smaller gain than low-order ones. The maximum spatial frequency of interest at which the MTF should be evaluated is inversely proportional to the sub-aperture size. This is often also a quite small effect.

Being a refractive optic, the pyramid introduces chromatic aberration, the thicker the pyramid, the higher the aberration. A double pyramid, e.g. the one implemented in AGW for FLAO@LBT, has been proposed to allow for much larger vertex angles for the individual prisms, while keeping the beam divergence fixed. This is important because a very small vertex angle is difficult to be obtained, with a high sharpness. But this means also that the pyramid component becomes thicker. However, as it's done for achromatic lenses, two prisms with different glasses can compensate for the chromatic aberration [10]. If we want to stress this concept, we could go further: like Achromatic lenses are corrected to bring two wavelengths, typically red and blue, into focus in the same plane, Apochromatic lenses are designed to bring three wavelengths, usually red, green, and blue, into focus in the same plane. One could think to implement the analogous concept to the Pyramid, obtaining an Apochromatic pyramid.

4. Previous works results on Pyramid WFS

In the framework of comparing the performance of adaptive optics correction using natural or laser reference star, Rigaut and Gendron [11], starting from previous works from Noll [12] and Cubalchini [13], derived a general expression for the noise propagation coefficients of each Zernike mode in the case of a Shack-Hartmann wavefront sensor, to be applied to the noise which affects the slope measurement of each subaperture (Fig. 3).

This result, in which system spatial and temporal errors are neglected, leads to a global reconstruction noise which is proportional to the photon noise and related to the maximum radial order which can be corrected by a system ($Q=D/r_0$ where D is the system aperture and r_0 is the Fried parameter).

The work from Rigaut and Gendron has been considered as a gauging point in Ragazzoni and Farinato [3], in which the authors investigated the pyramid WFS sensitivity with respect to a SH in perfect closed loop conditions. In this configuration, if the sampling of the wavefront is the same for both the sensors and a geometrical approximation is assumed, the SH WFS performance is not changed with respect to the open loop one, while the pyramid WFS SNR experiences an increase, thanks to the spot size reduction. Starting from an analytical discussion about the effect of such a resizing on the tip-tilt estimation error, and introducing the Heisenberg uncertainty principle argument, the authors extrapolate the estimation of the error of the pyramid WFS, with respect to the SH, for a Zernike

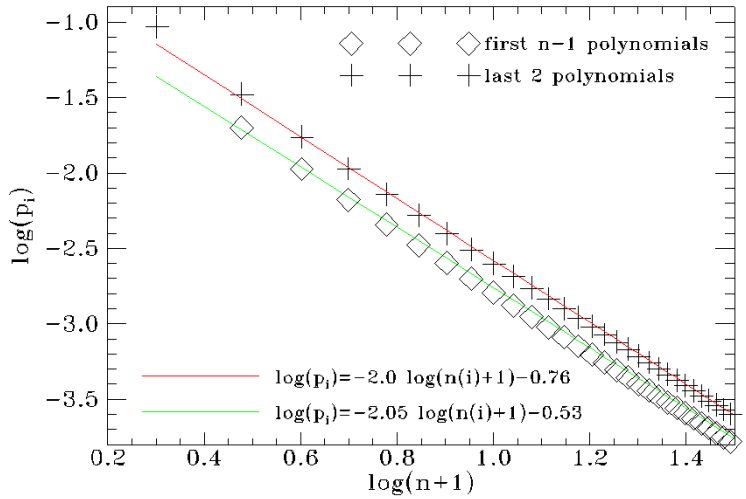

Fig. 3 noise propagation coefficients, as functions of the radial degree n, as computed in Rigaut&Gendron, 1992. (+) are of the last 2 polynomials, while (□) are for the first n-1 polynomials of each radial order. The linear fits shown on the plot slightly underestimate the error propagation coefficients for low modes (n < ~10).

polynomial of q^{th} radial order, resulting to be proportional to the SH error itself. As expected, for the highest modes the gain tends to zero. This dependence on the SH sensor variance allows the authors to assume that the same reconstructor is applied to both the WFSs and to use the noise propagation coefficients given in [11]. The resulting prediction was then proved for low radial orders (up to Q=7) with a laboratory experiment called *Pyramir*, as shown in Figure 2 (from [14]).

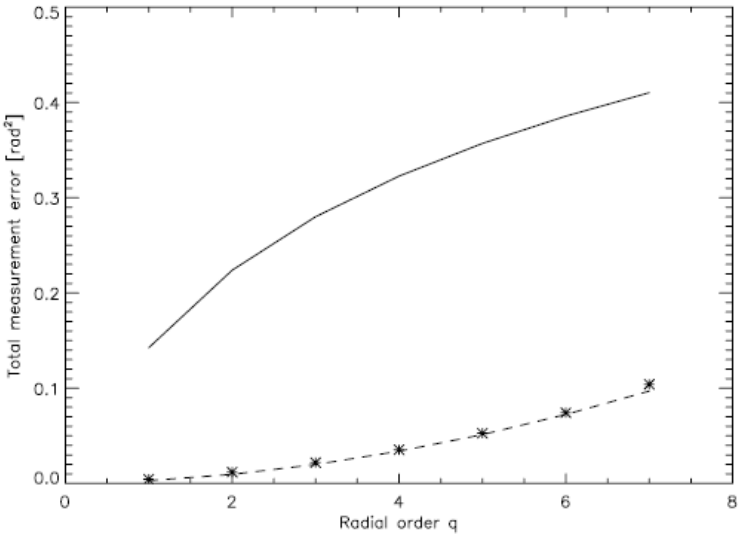

Fig. 4 Measurement error coefficient for a correction of radial order with maximum radial order Q = 7. Solid line marks the theoretical error of a SH wavefront sensor under the same conditions, dashed line denotes the predictions by Ragazzoni &Farinato (1999), asterisks show Pyramir measurements. (Peter et al. 2010)

The direct consequence of the lower propagation coefficients is a gain in terms of the limiting magnitude of up to 2.8 mag, for the next Extremely Large Telescopes generation, which can be achieved with a pyramid WFS with respect to a SH. This result has been differently quantified by Verinaud [15] with another model, resulting in a maximum gain in magnitude smaller by about 0.5 magnitude than Ragazzoni's result.

A compatible gain has been recently estimated by Esposito comparing the data from the FLAO system with analogous data taken with a different 8-m class telescope mounting a SH WFS, in similar seeing

conditions. The performance here increase thanks to a combination of the high ASM spatial sampling and the PWFS intrinsic gain. I must however recall that this comparison is only mainly qualitative for us: first of all we're speaking of different AO systems, second the details of the error sources involved in these two results are not completely known, so it's not easy to disentangle the actual Pyramid gain.

We can say that the overall gain in magnitude which results from [3] prediction can describe, in geometrical approximation, the actual pyramid gain but it only works in bright-end, since no assumptions on the effect of a Strehl Ratio lower than 1 on the pin of the pyramid have been considered.

5. Pyramid gain in limiting magnitude in between seeing and diffraction limits

To estimate the effect of a partial correction onto the pin of the pyramid, we approximate the shape of the re-imaged star as the direct sum of a seeing limited spot, produced by $(1- S)\times n^*$ photons, and a diffraction limited spot, formed by $S\times n^*$ photons, if n^* is the total number of collected photons. A simple analytic approach reveals the dependence of the pyramid wavefront sensor tip-tilt error on the Strehl Ratio value as still proportional to the SH variance, then, using the same argument on the Heisenberg uncertainty principle given in [3], which also assume that the sensitivity of the sensor is inversely proportional to the second power of the focal spot linear dimension, we can extrapolate the dependence of the propagation coefficients for the higher modes.

Fig. 5 shows the error propagation coefficients presented in [3] (black lines) for both the SH and the bright-end Pyramid cases. In the same Figure, the effect of different Strehl Ratios achieved on the pin of the pyramid in closed loop are compared: as one should expect, the difference between the performance of the SH and the Pyramid WFSs decreases for lower S values.

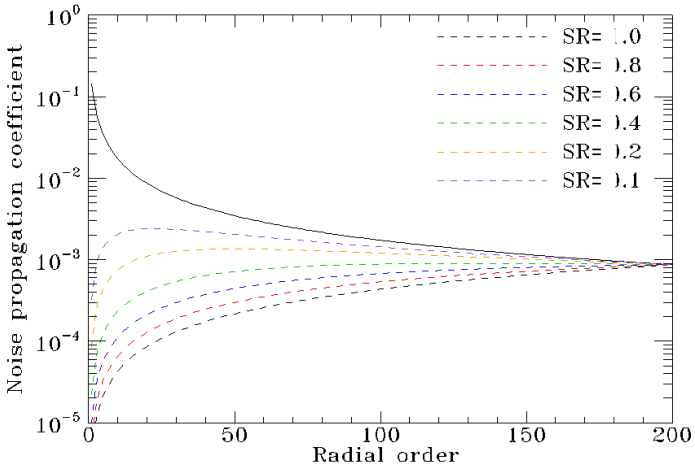

Fig. 5 Solid line: noise propagation coefficients vs the radial order q for the SH case; dashed lines: the same for the pyramidic case. Colors represent the effect of different S achieved on the pin of the pyramid in closed loop.

The resulting gain in terms of limiting magnitude, which is now dependent on the Strehl ratio, is shown in Fig. 6, for different values of $Q=D/r0$.

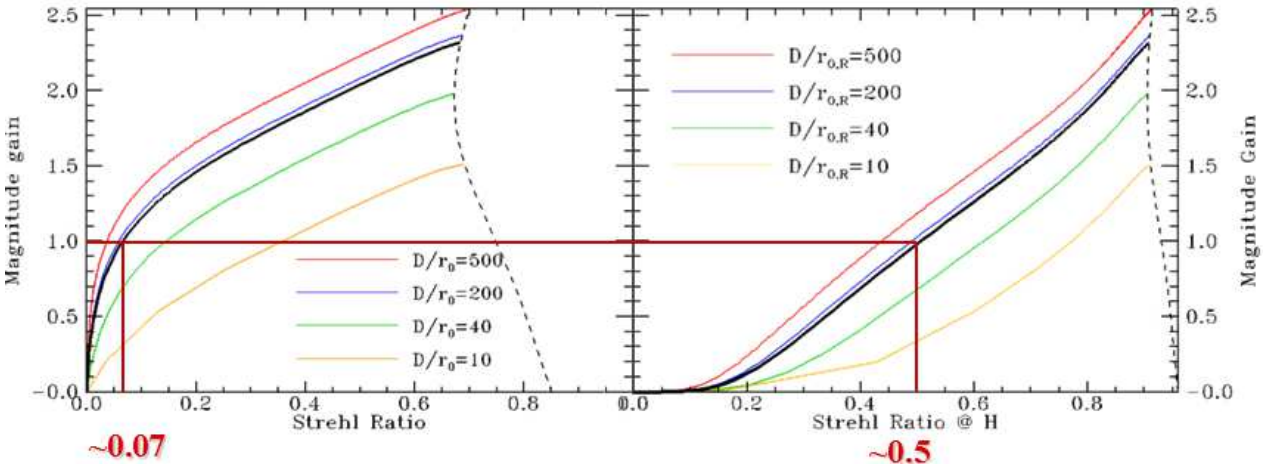

Fig. 6 the gain in limiting magnitude for different $Q=D/r_0$, as a function of the achieved SR on the pin of the pyramid. The dashed line shows the limit in the maximum *SR* which can be obtained for each Q-value. Right: same effect, if the sensing (Visible band) and the imaging (r_0 computed in the R-band) wavelengths are different. Black line corresponds to a E-ELT-like telescope, with a standard ESO Paranal 40-layers atmosphere.

As we can see, there's a limit on the maximum SR value which can be achieved, which is related to the maximum corrected radial order. As per [12], in fact, the residual root mean square error, after the correction of the first J (with J >10) Zernike modes of a wavefront perturbed according to Kolmogorov statistics, is known and translates into a limit Strehl ratio is given by the Marechal's approximation.

6. Non-linearity error issue

In this Section we analyze the behavior of the Pyramid wavefront sensor in terms of linearity, trying to quantify the non-linearity error associated to this type of WFS under typical atmospheric conditions. To reach this goal, we performed a full simulation with Fourier wave-optics propagation through a perfect Pyramid Wavefront Sensor, illuminating it with various kind of wavefront deformations (Zernike polynomials) and different amplitudes.

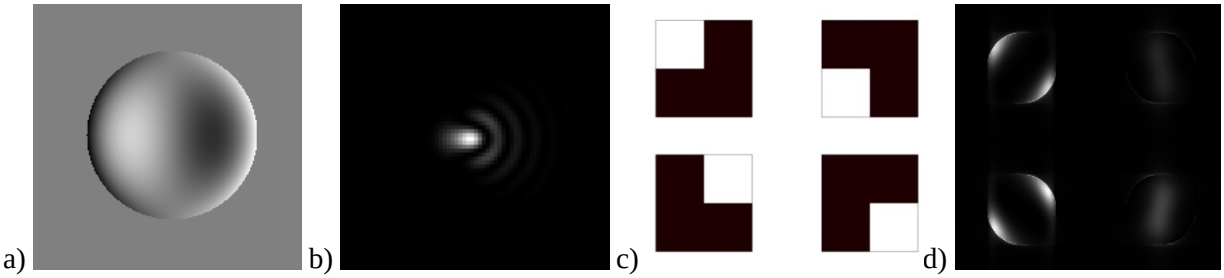

Fig. 7 Aberration Z^3_{-1} propagation through pyramid simulation steps: a) aberrated WF, b) PSF obtained from the electric field, used as a feedback, c) pyramid faces simulation, d) re-imaged pupils after pyramid.

The linearity of the sensor response has been quantified evaluating the range in which the retrieved aberration Z^i_j (recomputed using the Fast Fourier Transform integration method described also in [16] and fitting all the polynomials) deviates from the actually introduced one less than a certain threshold, in terms of RMS wavefront error. As a reference for the deviation, we considered the linear fit of the results obtained in a non-linearity-negligible regime. Fig. 8 shows the rms value of the input aberration for which the non-linearity error exceeds different threshold limits, ranging from 2.5% up to 20%.

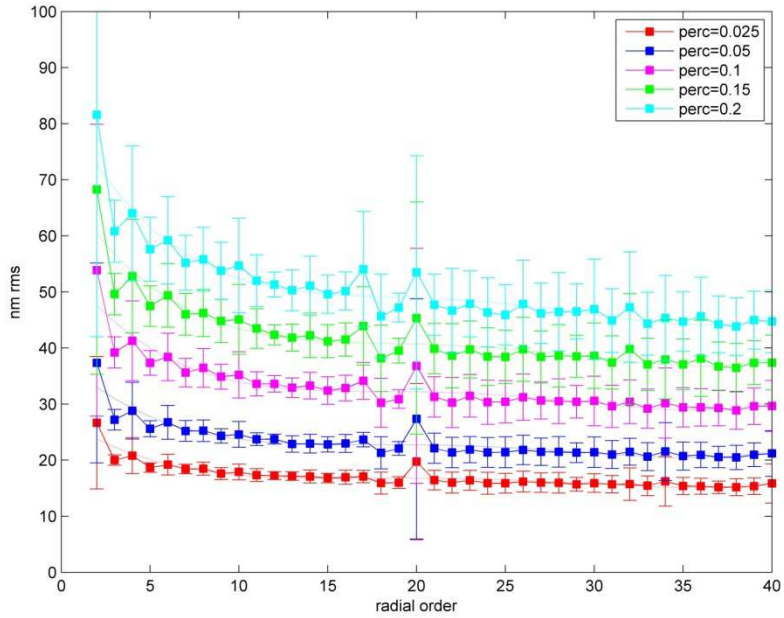

Fig. 8RMS amplitude (nm) of the input aberration at which the non-linearity error exceeds different threshold limits, ranging from 2.5% up to 20%, versus the radial order of the aberration. The bars represent the spread of this result which one can obtain for the different modes inside the considered radial order.

Looking at Fig. 8 one can see that the actual rms error due to non-linearity for a given mode can be estimated as a certain percentage of the input aberration amplitude, but the value of the percentage itself depends on the absolute input aberration too. If the coma aberration (radial order n=3) introduced, for example, is 60nm, than the coefficient of the Z^3_1 polynomial after the reconstruction will statistically deviate from the input value of about 20%, that is to say 12nm, but if the introduced amplitude is 40nm the expected non-linearity error reduces to 10%, i.e. 4nm. Moreover, since the single expected absolute value of the non-linearity error is related to the input aberration amplitude for each mode, it will follow the Kolmogorov statistics and depends on the actual atmospheric seeing. To obtain a global non-linearity error estimation, the contribution of all the modes has to be taken into account. We considered the 40 layers model of the Paranal atmosphere shown in Fig. 9, giving a total r_0~0.14m, an outer scale value of L=25m and an E-ELT-like telescope aperture D=40m (sensing wavelength λ=500nm) to compute, according to the Von Karman spectrum, a typical input value for each aberration mode. With these assumptions, the amplitude for a single (representative) polynomial of a radial order n can be assumed as the difference between the expected residuals of the correction of n and n+1 radial orders, divided by the number of modes in that radial order. The analytical expression for the rms residual error, computed in [12] for a pure Kolmogorov spectrum, has been extended to Von Karman spectra in [17].

Given these aberration amplitudes, an expected non-linearity error can be considered as the linearity deviation of each mode for that given amplitude, obtained linearly extrapolating from the curves in Fig. 8. The non-linearity error of each radial order has then been retrieved as the quadratic sum of the single modes. If we assume that the AO system is perfectly correcting the wavefront aberration up to a certain radial order n, the residual global non-linearity error can be estimated as the cumulative sum of all the non-linearity errors for radial orders larger than n (Fig. 10).

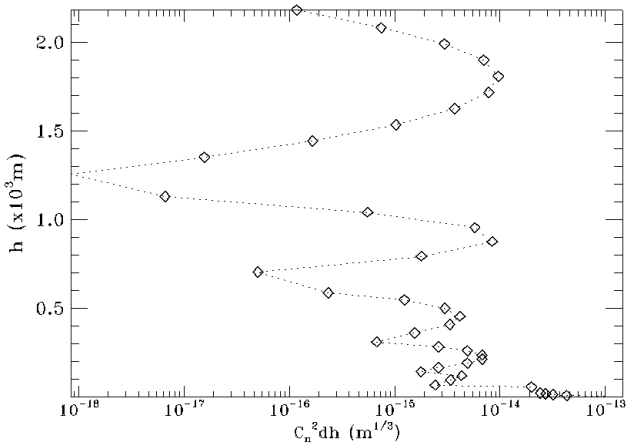

Fig. 9 Paranal 40-layers CN^2 profile model (reference) in the altitude-frequency plane.

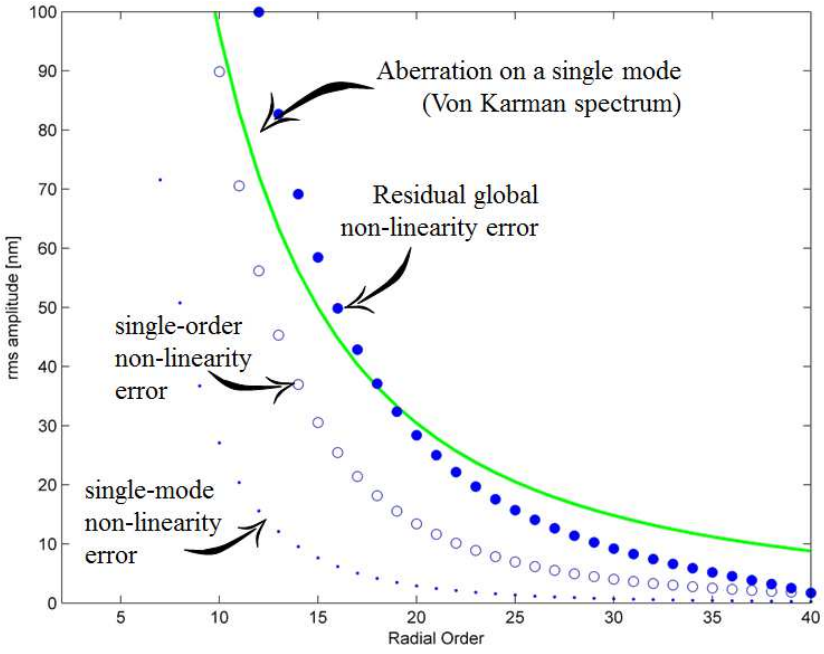

Fig. 10 Global non-linearity error estimation. *solid line:* expected aberration, for a single mode of each radial order, for the profile shown in Fig. 9 and a Von Karman spectrum; *small dots*: single-mode non-linearity error; *empty circles:* non-linearity error of each radial order; *filled circles*: residual global non-linearity error.

6.1. Effect of modulation

To estimate the effect of a circular modulation path of the pyramid onto the linearity error, we realized a new basis of *modulated Zernike polynomials*. For each mode, the pyramid modulation has been approximated with the sum of the average aberration measured by the pyramid WFS while the spot makes a circle on the pin of the pyramid, sampled with 8 positions (see Fig. 11).

Fig. 12 shows how the global non-linearity estimation, for each radial order (*filled red dots*), decreases in presence of a 3λ/D modulation. As expected, the error due to non-linearity is inversely related to the amount of modulation.

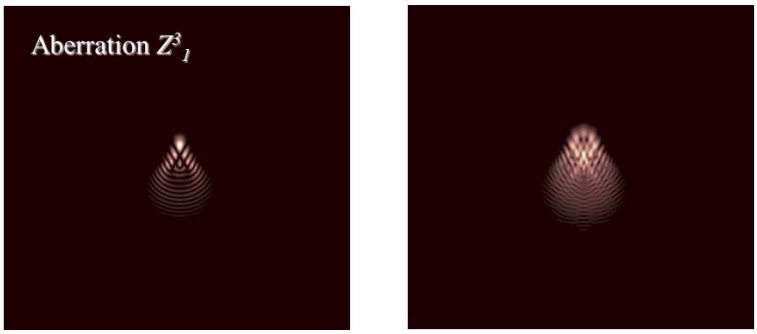

Fig. 11 Circular modulation on the pin of the simulated pyramid, for Zernike mode Z^3_1. Left: no modulation; right: modulation, with a 8-points sampling. This picture is used only for display purposes, since the average is done on the four re-imaged pupils, and not on the focal plane, to avoid interference patterns.

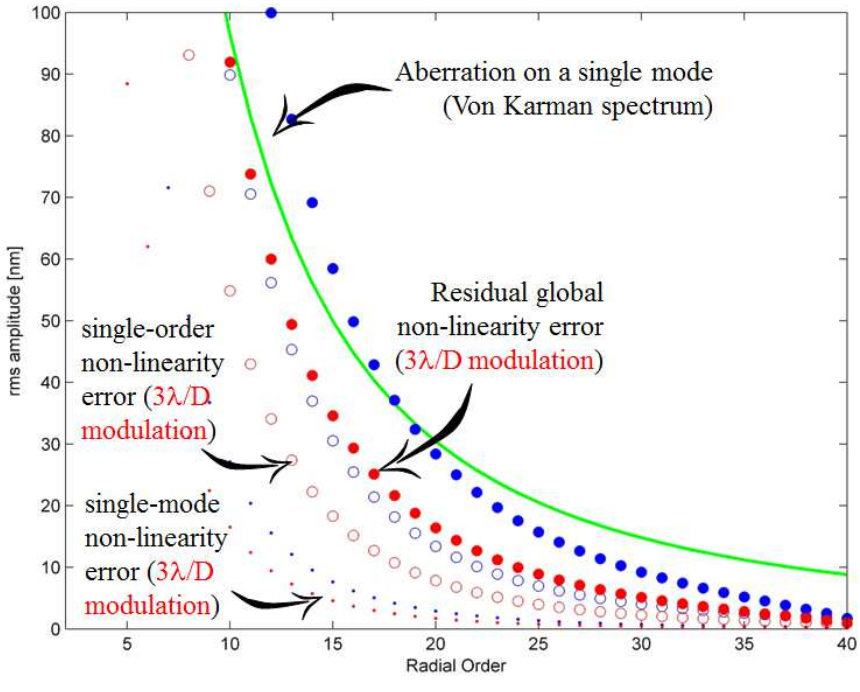

Fig. 12 Global non-linearity error estimation, considering also a 3λ/D modulation. *solid line:* expected aberration, for a single mode of each radial order, for the profile shown in Fig. 9 and a Von Karman spectrum; *small dots*: single-mode non-linearity error; *empty circles:* non-linearity error of each radial order; *filled circles*: residual global non-linearity error. *Blue dots*: without modulation; *red dots*: with modulation.

As it should be expected, the non-linearity error experiences a decrease when modulation is applied onto the pyramid. A further study on the optimization of these values for the E-ElT case is on-going.

7. Conclusion

The Strehl Ratio value on the pin of the pyramid, other than being <1 by definition, further decreases when the system works in open loop or the AO correction is limited to a FoV which does not include the reference stars. To estimate the effect of such a decrease on the sensitivity of a Pyramid WFS, we evaluated a model to approximate the PWFS gain in sensitivity with respect to a SHWFS under geometrical approximation in partial correction conditions.

Moreover, we described a non-linearity error model based on Fourier wave-optics propagation for PWFS which translates into a residual global error due to non-linearity, after a partial correction (in

terms of number of modes) and presented the first results of the implementation of an analogous model, in which modulation is introduced.

The work, however, is still on-going, since both these results are currently being studied in more detail.

8. References

1. R. Ragazzoni, J. Mod.Opt. 43, 289, (1999).
2. R. Ragazzoni, A. Baruffolo, J. Farinato, A. Ghedina, E. Marchetti, S. Esposito, L. Fini, P. Ranfagni, F. Bortoletto, M. D'Alessandro, M. Ghigo,G. Crimi, SPIE 4007, pp. 57-62, (2000).
3. R. Ragazzoni and J. Farinato, A&A, 350, L23, (1999).
4. S. Esposito, A. Riccardi, A&A, 369, L9, (2001).
5. E. Marchetti, R. Brast, B. Delabre, R. Donaldson, E. Fedrigo, C. Frank, N. Hubin, J. Kolb, J.L. Lizon, M. Marchesi, S. Oberti, R. Reiss, J. Santos, C. Soenke, S. Tordo, A. Baruffolo, P. Bagnara, CAMCAO Consortium, The Messenger, 129, 8-13, (2007)
6. J.M. Hill and P. Salinari, Proc. SPIE, 4004, 36-46, (2000).
7. R. Ragazzoni, C. Arcidiacono, M. Dima, J. Farinato, D. Magrin, V. Viotto, Proc. SPIE, 7736, 23-6, (2010).
8. D. Magrin, R. Ragazzoni, M. Bergomi, A. Brunelli, M. Dima, J. Farinato, V. Viotto, in AO4ELT2 Proc., p33, (2011).
9. E. Gendron, M. Brangier, G. Chenegros, F. Vidal, Z. Hubert, G. Rousset, F. Pouplard, AO4ELT conference, 5003, (2010).
10. E. Diolaiti, A. Tozzi, R. Ragazzoni, D. Ferruzzi, E. Vernet-Viard, S. Esposito, J. Farinato, A. Ghedina, A. Riccardi, Proc. SPIE, 4839, 299, (2003).
11. F. Rigaut and E. Gendron, A&A, 261, 677, (1992).
12. R.J. Noll, JOSA, 66, 207-211, (1976).
13. R. Cubalchini, JOSA, 69, 7, 972-977, (1979).
14. D. Peter, M. Feldt, T. Henning, S. Hippler, J. Aceituno, L. Montoya, J. Costa, B. Dorner, PASP, 122, 887, 63-70, (2010).
15. C. Verinaud, Opt. Comm.,233, 27-38, (2004).
16. F. Roddier and C. Roddier, Applied Optics, 30, 11, (1991).
17. D.M. Winker, JOSA, 8, 1568-1573, (1991).